Society of Petroleum Engineers

SPE-195866-MS

Overcoming Coring Challenges in a New Unconventional Play Offshore by Integration of Formation Evaluation Data

Thomas Bradley, Baker Hughes, a GE Company; Per Henrik Fjeld, Jonathan Scott, and Steven Ogilvie, AkerBP

This paper was prepared for presentation at the SPE Annual Technical Conference and Exhibition held in Calgary, Alberta, Canada, 30 Sep - 2 October 2019.

Abstract

A well was drilled into a prospective new unconventional mudstone play offshore Norway. Two of five coring runs were successful while the rest yielded little to no core recovery. Investigations attributed the poor recovery to sub-optimal coring practices, equipment failure and operational errors. Recently, the accompanying petrophysical logs and seismic data were revisited, and upon detailed investigation several unusual responses were observed to correspond with intervals of poor core recovery. Subsequent investigation of the core itself substantiated that the coring issues largely had natural causes. This understanding is being applied to two imminent coring operations and has driven selection of drilling, coring and wireline technology and procedures, in addition to informing casing design.

Wireline nuclear magnetic resonance (NMR) and cross dipole acoustic data, logging whilst drilling (LWD) density (including azimuthal images), neutron porosity and resistivity was acquired over the interval of interest for standard formation evaluation purposes. This interpretation was conducted immediately after the initial drilling and showed the formation to be a series of highly porous oil bearing mudstones. However, no in depth advanced interpretation was conducted at the time. Recently, advanced analysis including high resolution log enhancement, NMR 2D porosity and saturation analysis, acoustic azimuthal anisotropy, near wellbore imaging, fracture interpretation, and borehole image interpretation were performed on the log data, and new and improved 3D seismic data was interpreted. When interpreted in detail it could be observed that unusual responses in the logs showed a close correspondence to the intervals of poor core recovery. In particular, high azimuthal anisotropy was observed, and when this was compared to the near wellbore reflection image a significant planar reflecting feature was identified which is determined to be a fault. Indications of this feature was subsequently found in seismic data. When then compared to the azimuthal density image after resolution enhancement was applied, although the image is still of too low resolution to directly image the fault, disturbed bedding was observed which is commonly associated with faulted intervals. Several core fragments proved to have extensive small-scale fracturing not noticed previously, and slickenlines were found along several larger fractures previously presumed to be drilling induced.

The investigations of the log data revealed that a previously unknown sub-seismic fault was present right below the depth where coring problems were encountered. The detailed interpretation was able to determine the precise location of the fault and its extent in the formation. Knowledge of this subsequently explained

the coring problems encountered and helps to optimise imminent coring in the same formation. Lessons learned and the methodology likely also applies to similar formations.

In this paper we discuss coring issues encountered in a new and unconventional play offshore, present new data and interpretation that sheds light on them and describe the methodology of the detailed integrated interpretation that uncovered the previously unknown root cause. We then discuss how these findings can be (and are) used to optimise both drilling, coring, and logging operations in future wells.

Introduction

The Valhall Field, located in Block 2/8 of the Norwegian North Sea. The primary reservoir is Cretaceous chalk, located at approximately 2400m TVD. Production of this reservoir started in 1982. Above this are various other formations – in particular a shallower potential unconventional mudstone reservoir.

Figure 1 shows the location of the Valhall field:

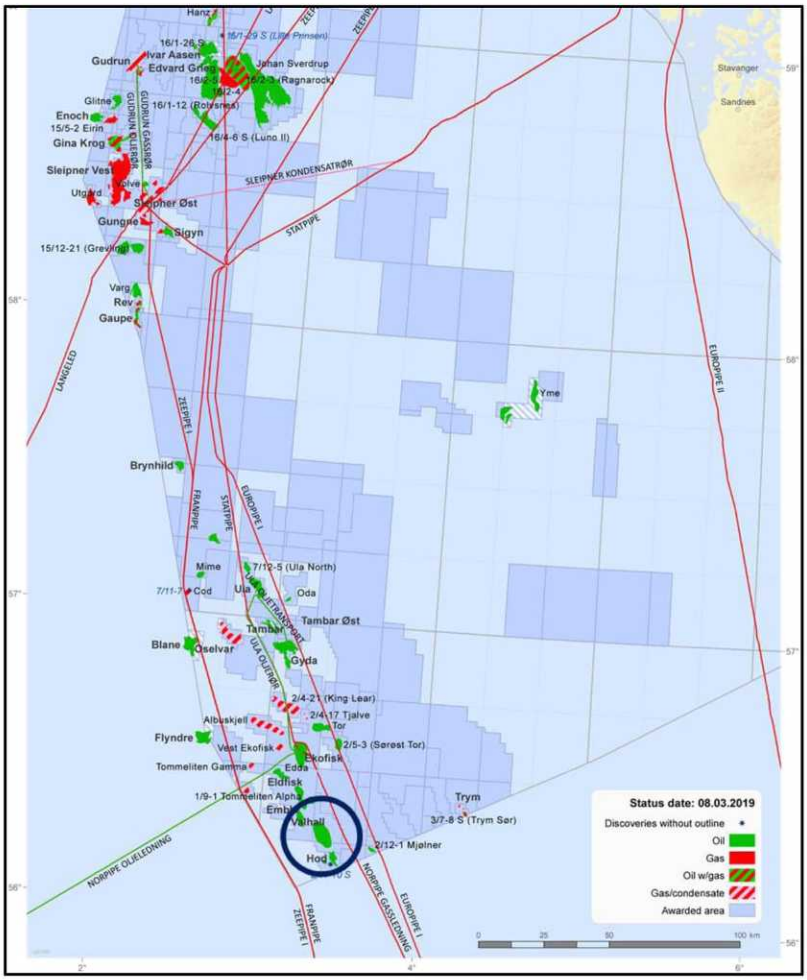

Figure 1—Location of the Valhall field, circled in dark blue (from www.norskpetroleum.no)

A production well was drilled targeting the Cretaceous chalk reservoir. As part of the drilling program LWD and wireline logs (including, LWD density, neutron, gamma ray and acoustic, and wireline spectral gamma ray, cross dipole acoustic, nuclear magnetic resonance, and formation testing and sampling) were run across the potential mudstone reservoir to appraise the standard petrophysical properties (for example lithology, porosity, water saturation etc.). A conventional core was also attempted, however recovery was poor with repeated jams being encountered.

Coring Challenges

During coring operations, significant problems were encountered when coring the mudstone intervals. Because of frequent jams core recovery was poor. Table 1 presents the coring summary table highlighting where coring issues were encountered.

Table 1—summary of cored intervals

Core Number	Top Cored Interval Metres MD	Base Cored Interval Metres MD	Comments
1	xx88.1	xx06.3	
2	xx06.3	xx33.5	Start of poor recovery and rubble zone
3	xx33.5	xx60.5	No recovery
4	-	-	No recovery – equipment issues
5	xx60.5	xx87.5	

This is illustrated in Figure 2 which shows a section of the core from xx14 m, showing the typical condition of the recovered core when still in the core barrel.

Figure 2—Core photo of core 2 at xx14m. Considerable apparent damage can be observed in the core.

At the time of operations, poor recovery was attributed to coring practices employed and no further coring was attempted.

Formation Evaluation

The mudstone interval was not a primary target for the well. Therefore, limited formation evaluation of these intervals were carried out: mainly to estimate the petrophysical properties (lithology, porosity, water saturation etcetera). However, at the time of initial logging the more advanced formation evaluation data (such as images, full waveform acoustic, and nuclear magnetic resonance data) was not fully evaluated.

A few years after initial operations, the log data was revisited – in particular detailed interpretation was conducted of all the recorded log measurements, including:

- Log data resolution enhancement, including enhancement of LWD bulk density and gamma ray images to enhance imaging of smaller scale features
- High resolution volumetric analysis for lithology, porosity and saturation quantification.
- Comprehensive NMR porosity and saturation analysis to estimate bound and moveable water volumes, and hydrocarbon filled porosity.
- Integration of NMR and conventional log data to further quantify moveable versus non-moveable water and hydrocarbon volumes.
- Borehole image analysis for structural analysis around the wellbore
- Acoustic analysis to estimate stress distribution around the wellbore, fracture evaluation, and acoustic reflection imaging to visualize the structure up to 5 metres from the wellbore.

On examination of the results over much of the interval, the integration of the conventional and advanced volumetric measurements gave considerable extra value in assessing the petrophysical properties of the mudstone. However detailed discussion of these results is outside the scope of this paper.

In addition to the extra information gleaned from the advanced volumetric interpretation, over certain intervals, some rather unusual log responses and interpretation results were seen which were deemed worthy of further investigation. These include:

- Local variations from the overall trend in acoustic azimuthal anisotropy.
- Local radial variation of shear slowness with distance from the borehole that is not present immediately above and below.
- Localised disturbance in bedding seen on high resolution bulk density and gamma ray images.
- Change in frequency and amplitude character of monopole and dipole acoustic waveform data.
- A noticeable very high amplitude reflective feature present in the near wellbore reflection image.

As all these observations occurred at a similar depth, it is unlikely these can be attributed to issues with the log responses (for example tool issues or borehole effects on the log measurements). Each of these will now be discussed in turn.

Figure 3 presents the acoustic azimuthal anisotropy analysis over the interval of interest:

The log presentation for figure 3 is as follows:

- Track 1 – gamma ray, borehole deviation, tool azimuth, calliper and bit size.
- Track 2 – depth, and rose diagram showing fast shear direction for each 25m interval.
- Track 3 – azimuthal anisotropy (in green) measured over the tool 3.5ft receiver array length, and average anisotropy (in black) measured over the tool 10.5ft transmitter to receiver spacing.
- Track 4 – image presenting radial acoustic anisotropy around the borehole with edge of image oriented to geographic north. Shading intensity indicates degree of anisotropy, with lighter shading indicating higher anisotropy.
- Track 5 – fast shear azimuth direction and uncertainty (indicated by black shading).

Over much of the interval, the fast shear orientation is consistently oriented approximately north west-south east which suggests a predominant north west-south east principal stress direction. However over the interval from xx29m to xx35m a noticeable perturbation in the anisotropy orientations and magnitudes can

be seen, which also corresponds with a change in the character of the calliper curve. These perturbations suggest that a localised feature resulting in a change in the azimuthal anisotropy orientation may be present.

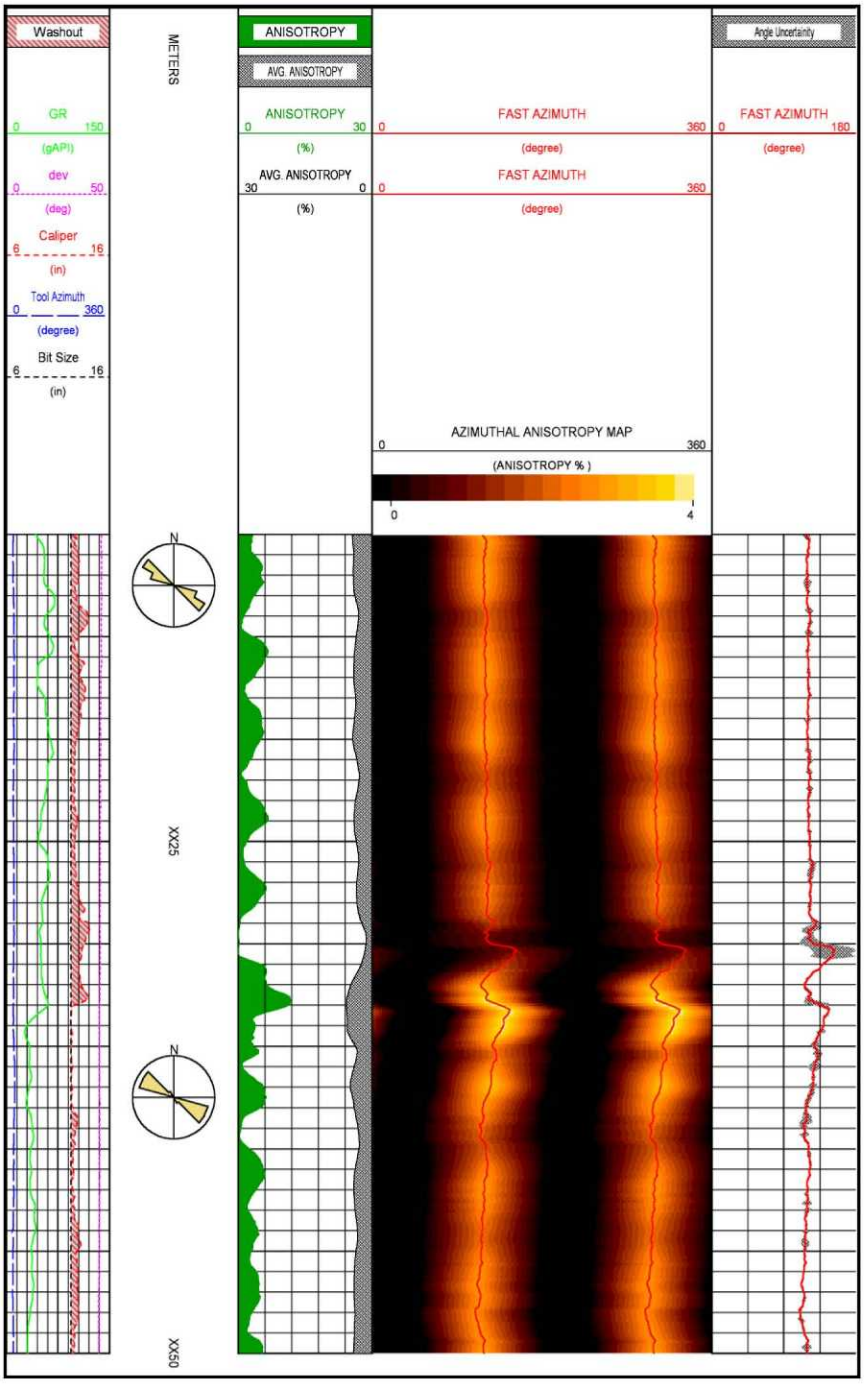

Figure 3—azimuthal anisotropy analysis results. Refer to text for detailed description of figure

Figure 4 shows the logged and enhanced density image over the interval of interest: The log presentation for figure 3 is as follows:

- Track 1 – gamma ray, calliper.
- Track 2 – depth

- Track 3 – bulk density image as logged
- Track 4 – resolution enhanced bulk density image

Over much of the image (Figure 4), the indications are that low angle to borehole planar bedding is present. However over the interval from xx33 to xx38m this trend changes. Because of the relatively low resolution of LWD bulk density images compared to other imaging technologies (even after resolution enhancement) the individual beds cannot be seen, but the general image character indicates disturbance in the bedding compared to above and below. This corresponds with the change in the azimuthal anisotropy direction from the overall trend observed in the azimuthal anisotropy analysis; therefore a further line of evidence to the presence of a localised structure.

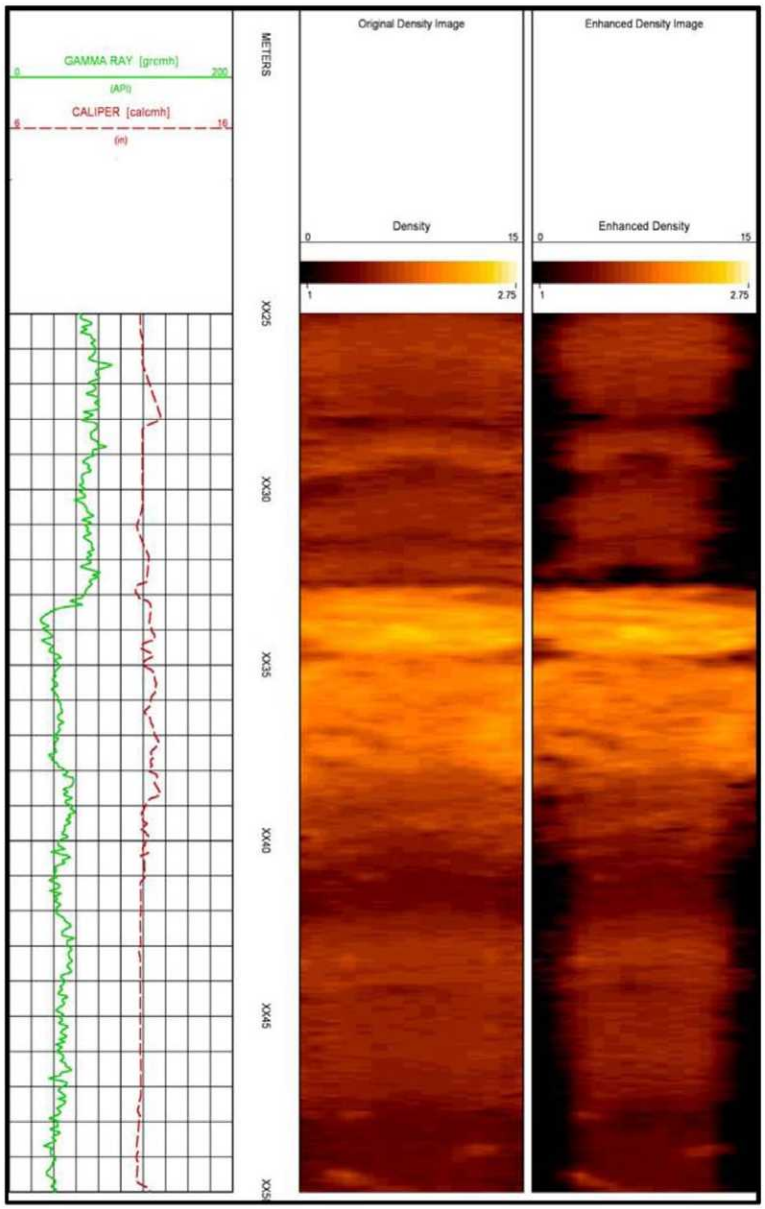

Figure 4—logged and enhanced density image. Refer to text for detailed description of figure

Further evaluation of the acoustic waveform data allows the radial variation of shear slowness with distance to the borehole to be evaluated. This is presented in Figure 5:

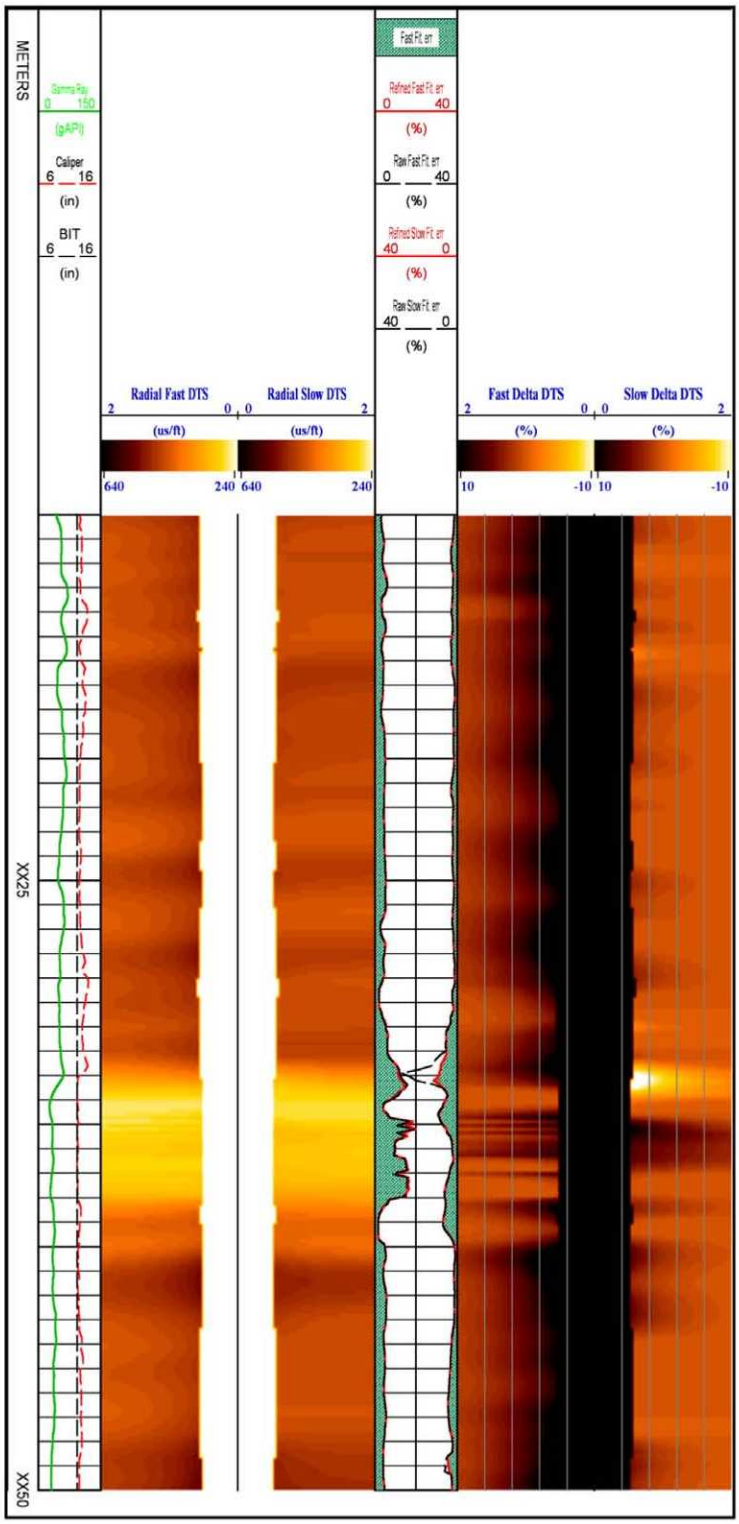

Figure 5—radial variation of fast and slow shear with distance from the borehole. Refer to text for detailed description of figure

The log presentation for figure 5 is as follows:

- Track 1 – depth.
- Track 2 - gamma ray, calliper, bit size.

- Track 3 – image of shear slowness versus distance from borehole, with borehole in centre and track edges representing 2ft from borehole axis. Left hand image represents variation in fast shear and right hand image variation in slow shear. Colour scaling indicates shear magnitude with lighter being faster.
- Track 4 – measured and modelled shear fitting inversion misfit: Fast misfit plotted in left of track and slow misfit on right of track.
- Track 5 – image of relative variation in shear slowness with distance from borehole, with borehole in centre and track edges representing 2ft from borehole axis. Left hand image represents fast shear and right hand image slow shear. Colour scaling indicates percent difference in magnitude, with light shading indicating decreasing slowness (i.e. faster formation).

Again, over much of the interval the radial variation in shear is relatively consistent. Once the large variations in shear slowness near to the wellbore (most likely associated with the near wellbore damaged zone) are passed, few changes in the slowness distribution away from the borehole with depth are observed. However over the interval xx33 to xx39m a noticeable change in the radial variation trend can be seen that does not follow the trend above and below. Again this correspondence with the other data suggests that a localised feature with significantly different properties to the surrounding formation is present.

The wireline acoustic data was then further analysed to generate a near wellbore reflection image using shear waves reflected from planar features in the formation. In this formation, imaging features extending up to five metres from the borehole axis is possible. As part of this, a three dimensional image investigating the 360 degree volume round the borehole was generated, to fully visualise the formation round the wellbore.

Four planes from the three dimensional radial reflection image are presented in figure 6:

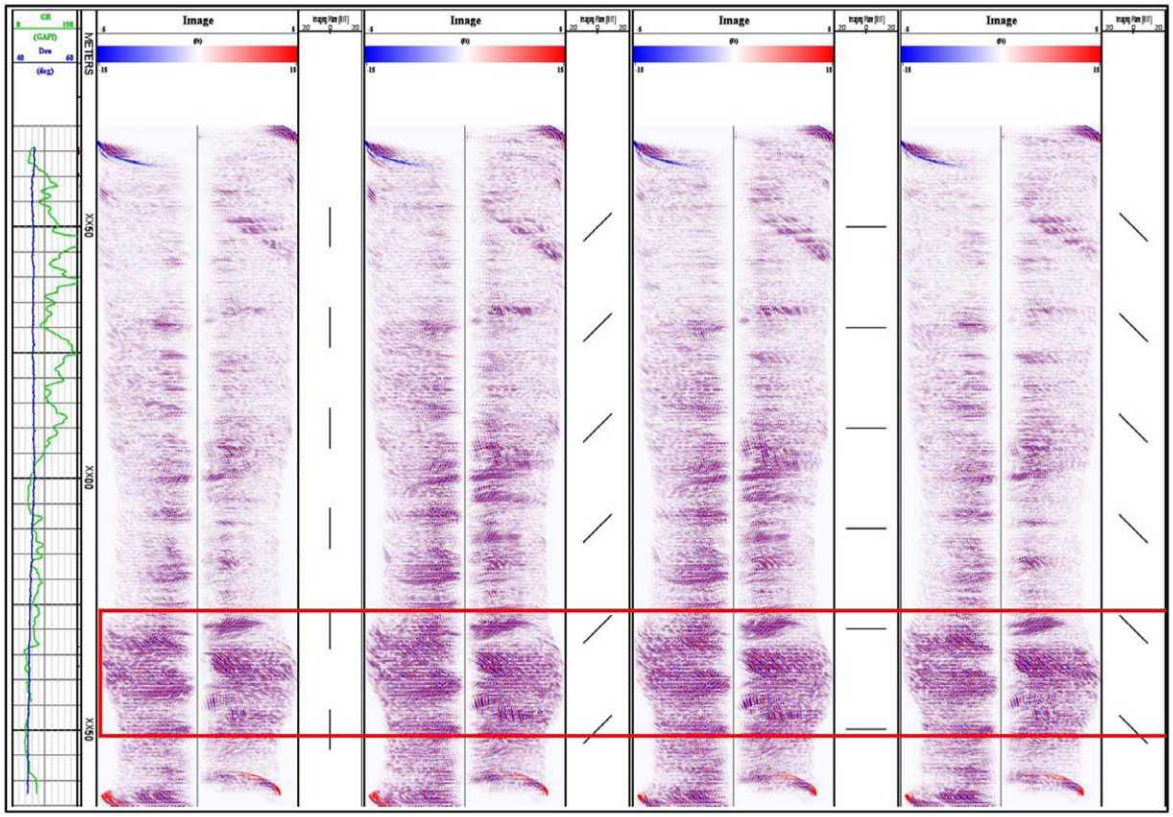

Figure 6—radial shear reflection images at zero, 45, 90 and 135 degrees. Refer to text for detailed description of figure

The display is as follows:

- Track 1 – gamma Ray, borehole deviation.
- Track 2 – depth.
- Tracks 3,5,7,9 – reflection images plotted at imaging plane orientations of zero, 45, 90 and 135 degrees to north, with the borehole in the centre of the image, and the track edges representing a distance of 5 metres from the borehole.
- Tracks 4,6,8,10 – sticks indicating orientation of imaging planes.

The images display reflections from planar features in the formation. Of particular interest is the strong reflection present intersecting the borehole at approximately xx35m (highlighted by the red box). As this can be observed to a certain degree in all planar orientations, this suggests that a very high acoustic impedence contrast is present between the reflecting feature and surrounding formation.

High acoustic impedence contrasts are commonly associated with structural features such as fluid filled fractures and faults. The amplitude of the reflection here suggests that the feature has a large aperture, or has a significant damage zone either side of the feature, hence strongly suggesting that the reflecting feature is a fault.

Data Review

Indications from analysis of the advanced measurements are that over the approximate interval xx30 to xx40m a localised change in the formation is present, although the initial indications from the available logs at the time of drilling were somewhat unclear what may be causing this.

Figure 7 presents a composite plot of the analysis described above where the various results are combined and compared to the cored intervals.

The tracks on the plot are as follows:

- Track 1 – depth
- Track 2 – LWD (green) and wireline (blue) gamma rays, LWD calliper.
- Track 3 – high resolution enhanced LWD density, neutron, and wireline compressional slowness.
- Track 4 – LWD resistivity data processed for fixed depths of investigation and vertical resolution.
- Track 5 – azimuthal anisotropy analysis map.
- Track 6 – enhanced resolution LWD density image.
- Track 7 – radial shear slowness profile, fast shear on left, slow shear on right.
- Track 8 – radial delta shear slowness profile, fast shear on left, slow shear on right.
- Track 9 – shear reflection image with imaging plane oriented at 45 degrees/135 degrees to north.
- Track 10 – cored interval indications, green shading corresponds to core 2, red to core 3.

Over much of the interval, where core recovery was better, the formation properties can be seen to be relatively consistent with little variation. However, this is not the case in all intervals. Of particular interest is the interval from xx33 to xx39 m which is where core recovery was poorest, and associated with this poor recovery, a significant change in all the various measurements can be observed that is not consistent with the formations above and below. When all measurements are compared to the core it can be clearly seen that this corresponds to the interval where the cores are showing significant l ocalised damage and poor recovery. The rugosity on the calliper cannot alone explain the observed log responses.

This correspondence can be seen to be more than coincidental, and strongly suggests that the coring issues experience cannot alone be attributed to poor coring practices, and that localised changes in the formation properties as indicated by the logs, can possibly be identified as a probable cause.

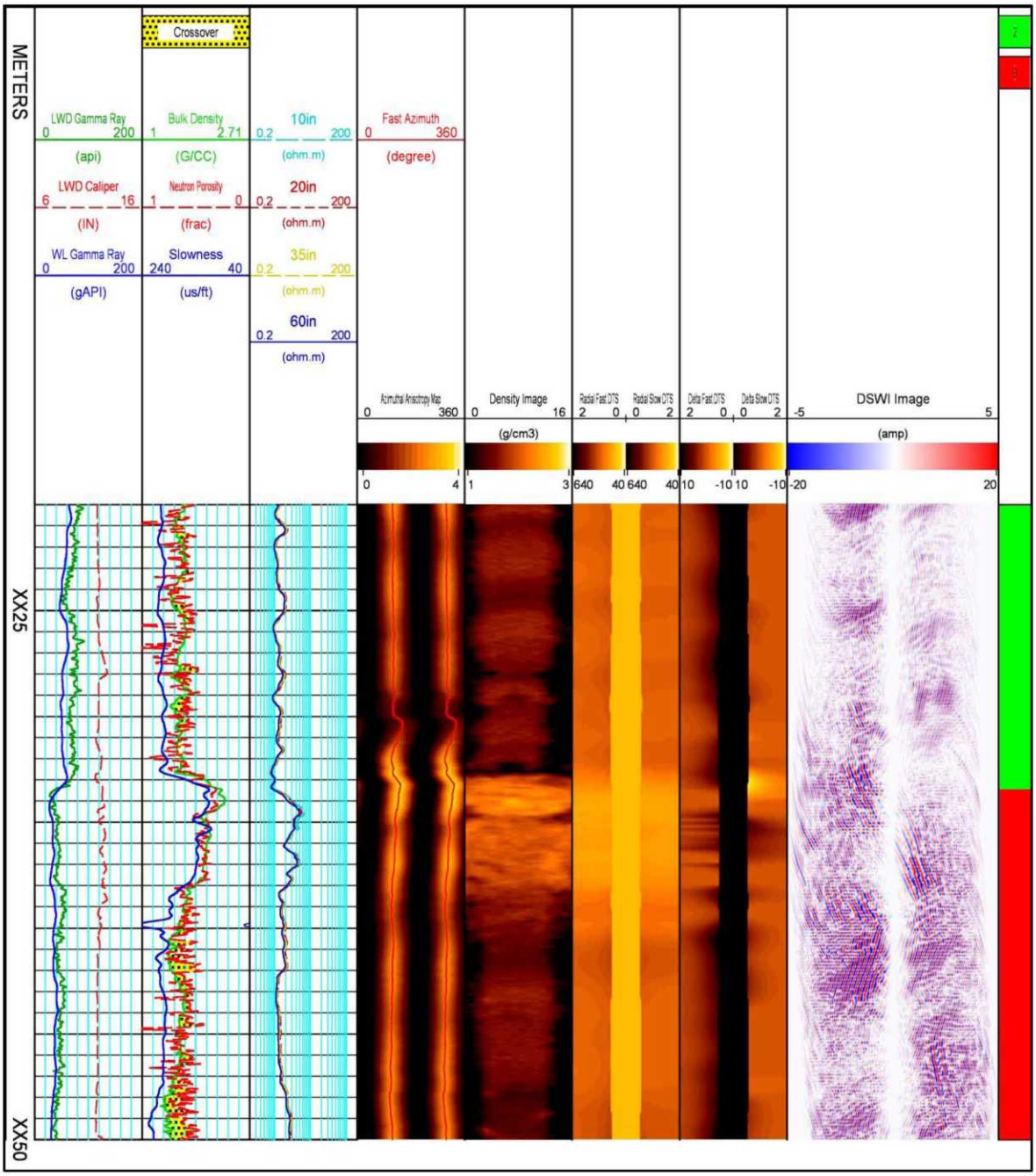

Figure 7—summary presentation comparing various interpretation methods over the interval of poor core recovery. Refer to text for detailed description of figure

Comparison with Seismic and Other Information

The well penetrates a mapped fault at approximately the location of a circa 19m long rubble zone (from circa xx08 to xx27 m) observed in the core (as shown in Figure 8).

Figure 8—Photo of core from 19m long rubble zone from xx06.5 to xx25.5m (core 2)

Close inspection of the rubble shows that each piece or pod was originally surrounded by black hairline fractures. The coring process dislodged most of these pods. Some have remained intact: for example the small pods surrounded by black hairline fractures at the left hand side of the piece of rubble as shown in Figure 9.

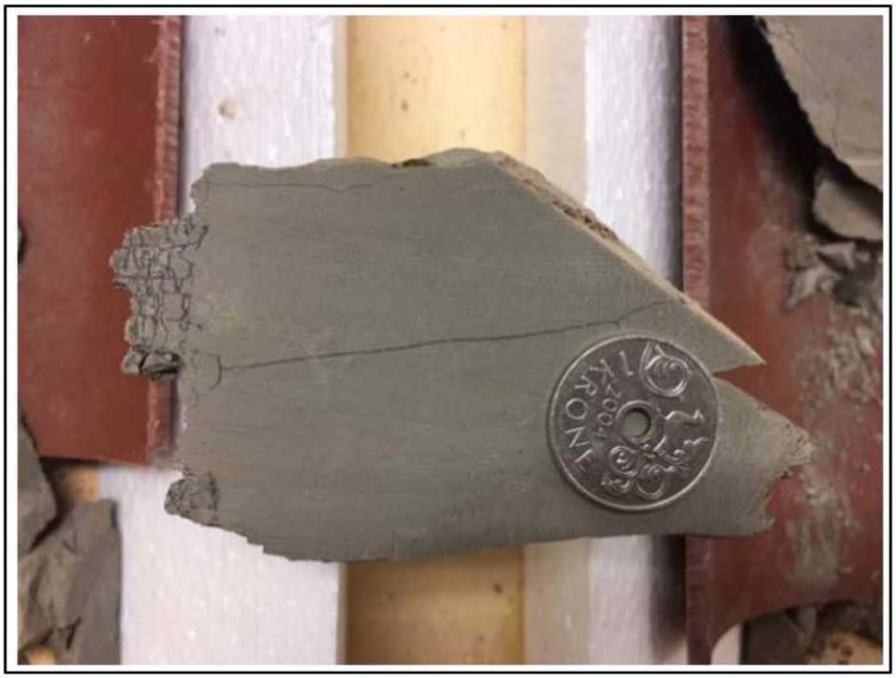

Figure 9—close up of one pod from core 2, showing black hairline fracture

It is likely that the rubble zone extends beyond the cored section based upon the logging evidence already presented. Potentially to at least xx40 m MD. Deeper in the cored section (at xx82 m MD), an 8m zone of discrete fractures with well-developed slip planes and slickenlines are present (as shown in Figure 10).

Figure 10—slickenlined shear fracture deeper in the cored section

This is considered to be a damage zone related to the fault identified in the seismic data.

These observations from core are supported by the observations from the log data: the depths of the unusual log responses show a close correlation with the considerable damage and brecciation observed on the core, hence suggesting that the reason for these responses and observations is the presence of a fault.

These observations of fault-related fracturing fit the conceptual model of Johri et al (2014) relatively well, as illustrated in figure 11. Although clearly further data (from additional wells) is required together with testing the production potential of these structures. A relatively impermeable fault core is surrounded by a highly fractured damage zone in a fractured, low permeability matrix reservoir. Oil and gas from the host rock will drain into the fault zone.

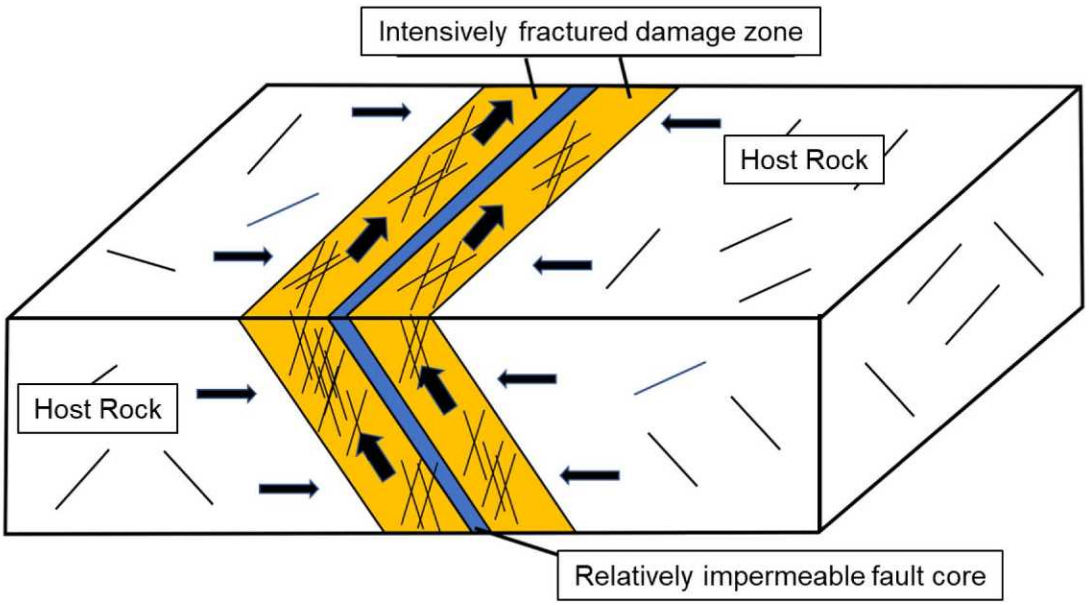

Figure 11—Conceptual model of a fault zone as penetrated by the well. Modified from Johri et al (2014).

Conclusions

Commonly when coring issues are experienced, this is attributed to coring practices not being followed. Although the effect of formation properties on coring is known it is not often considered in the final assessment of a coring program. In this paper we have shown that when coring challenges are experienced, analysis of the formation evaluation data from the well can often be used to explain the challenges experienced – in this case identifying the presence of a previously unknown sub-seismic fault. Furthermore, detailed evaluation of the formation evaluation data can then assist in the planning and execution of future coring operations in similar formations, so as to ensure optimal core recovery and operational success.

Acknowledgements

The authors would like to thank AkerBP ASA for releasing the data used in this paper, and AkerBP ASA and Baker Hughes, a GE Company for their support in publishing this paper.

References

Bradley, T. [2018] US Patent Application ACW4-64896-US-PSP Directional Near Wellbore Imaging Visualization.

Hornby B. E. [1989] Imaging of near borehole structure using full-waveform sonic data: *Geophysics*, volume **54** number 6, 747–757.

Johri, M, Zoback, M.D, Hennings, P. 2014. A scaling law to characterize fault-damage ones at reservoir depths. *AAPG Bulletin*, V.**98** (10), p 2057 – 2079.

Tang, X. Zheng, Y. Patterson, D. [2007] Processing array acoustic-logging data to image near-borehole geologic structures: *Geophysics*, volume **72** number 2, E87–E97.

Tang, X., Chunduru R., 1999: Simultaneous inversion of formation shear-wave anisotropy parameters from cross-dipole acoustic-array waveform data: *Geophysics*, volume **64** number 5, 1502–1511.

Tang, X. Zheng, Y. Patterson, D, 2010, Mapping Formation Radial Shear-Wave Velocity Variation By A Constrained Inversion Of Borehole Flexural-Wave Dispersion Data, *Geophysics*,Vol. **75**, No. 6 November-December 2010

www.norskpetroleum.no, Southern North Sea Overview map. Retrieved from https://www.norskpetroleum.no/wp-content/uploads/2-Felt_funn_Nordsj%C3%B8en-E-20032019.png 20th June 2019